Local control of spin flow in weak magnetic fields

J.-H. Quast, G. V. Astakhov,* W. Ossau, and L. W. Molenkamp
Physikalisches Institut (EP3), Universität Würzburg, 97074 Würzburg, Germany

J. Heinrich, S. Höfling, and A. Forchel
Physikalisches Institut (TP), Universität Würzburg, 97074 Würzburg, Germany

(Dated: October 24, 2008)

We demonstrate that optical illumination strongly influences spin transport in n-type GaAs. Specifically, increasing the power density of optical spin pumping results in a significant expansion of the spin diffusion profile. A further means of manipulation is the application of a weak transverse magnetic field, which strongly increases spin flow out of the excitation spot. These effects are directly monitored in spin imaging experiments and spatially resolved Hanle measurements.

PACS numbers: 72.25.Dc 72.25.Fe 85.75.-d 72.25.Rb

The ability to monitor, control and manipulate spin flows in semiconductors is a prerequisite for the functionality of spin-based devices. Because of the spin-selectivity of the selection rules [1], optical spectroscopy has emerged as a powerful tool to locally probe the spin of electrons. Spin diffusion lengths of over ca. 10 μm in n-GaAs [2] and spin drag over 100 μm [3] enable optical detection of spin injection [4, 5, 6, 7, 8], spin accumulation [7] and the spin Hall effect [9]. In this type of experiments, the optical excitation density is kept low in order to minimize a possible perturbation of the spin system, implicitly assuming that using a low optical power density implies that the dilution of the intrinsic electrons in the semiconductor with photo-generated ones can be neglected. Generally, this condition is met when $G\tau < n_e$, where G is the generation rate (which is proportional to the illumination power density), τ is the lifetime of the photo-generated carriers and n_e is the concentration of intrinsic electrons. However, for a spin polarized electron system, recombination with photo-generated holes will reduce the spin polarization. This additional effect becomes relevant when $G\tau_s > n_e$, where τ_s now is the electron spin relaxation time [1]. Therefore, in semiconductors with a very long electron spin memory, i. e., when $\tau_s \gg \tau$, this mechanism may lead to enhanced spin decay at quite low pump/probe power densities, and hence should not be neglected a priori. On the plus side, this same mechanism can be used to locally control spin flow even without application of a bias voltage, as we will demonstrate below.

We present results for a Si-doped n-type GaAs layer ($n_e = 2.5\times10^{16}$ cm^{-3}) of $d = 1.5$ μm width. It was grown by molecular-beam epitaxy (MBE) on semi-insulating (001) GaAs substrate followed by an undoped 200 nm GaAs buffer, a 5 nm AlAs barrier and an undoped 100 nm GaAs spacer layer. The sample is mounted strain-free and kept at a temperature $T = 8$ K. In order to perform optical spin pumping and probing we use a two-color Kerr rotation technique [10]. Optical excitation is performed by a solid state laser (785 nm) modulated between σ^+ and σ^- circular polarizations at a frequency of 50 kHz. The net spin polarization along z direction S_z is probed using the magneto-optical Kerr effect (MOKE). The photoinduced Kerr rotation θ of a Ti:sapphire laser (819 nm) which is proportional to the spin polarization ($\theta \propto S_z$) is measured by balanced photodiodes and demodulated by a lock-in amplifier. Scanning Kerr microscopy is used to spatially resolve the net spin polarization [3, 11]. In this technique, a circularly-polarized pump beam is directed under a 45° angle of incidence to the sample surface. After refraction inside the sample the pump beam generates spins polarized at an angle $\gamma = 11°$ with respect to the sample normal (z direction). Surface scans in the x-y plane are performed using a microscope objective (NA = 0.14) mounted on a piezo system. Another microscope objective is used to focus the pump beam.

First, we characterize the sample in an excitation configuration where spin diffusion is averaged out (Fig. 1), using two-color Kerr and photoluminescence (PL) measurements. Instead of the microscope objective, we employ two long-focus lenses to provide spot sizes of about 100 μm, much larger than the typical spin diffusion length. The PL spectrum consists of two bands which we attribute to donor-acceptor (D^0, A^0) transitions and donor-bound excitonic (D^0, X) recombination [see Fig. 1(a)]. In the same Figure, we plot with the optically induced circular polarization ρ_c of the PL [detected at (D^0, X) band], as function of the excitation energy. A maximum value of $\rho_c = 22\%$ (the theoretical limit is 25% [1]) is achieved for quasi-resonant excitation. The vertical arrow in Fig. 1(a) indicates the pump energy $E_0 = 1.58$ eV which will be used in all further experiments. The PL circular polarization is proportional to the net spin polarization, $\rho_c = S_z/2$. Its amplitude depends on pump power; ρ increases linearly for low- and saturates for high pump power density, as shown in Fig. 1(b). This behavior can be well described by [1]

$$S_z(W) = \frac{S_{z0}}{1 + W_S/W} \qquad (1)$$

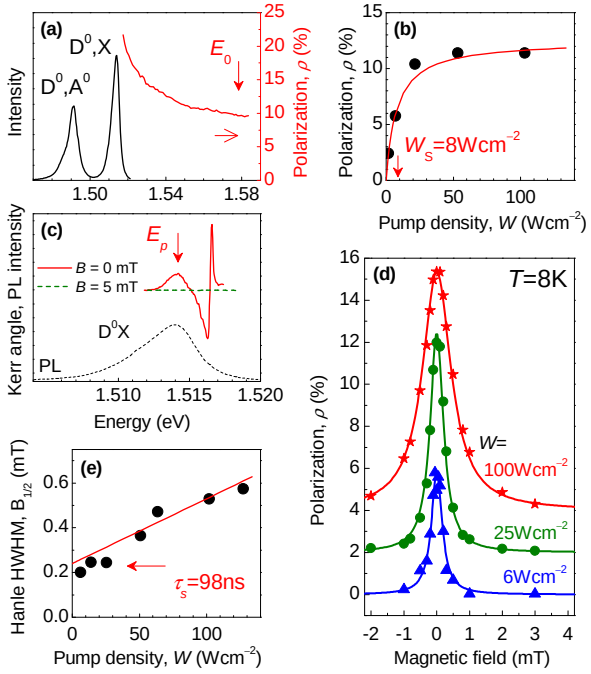

FIG. 1: (Color online) Sample characterization in a configuration where spin diffusion is averaged out. (a) PL and polarization excitation spectra. (b) PL polarization vs. pump power density. Solid line is a fit to Eq. (1). (c) Kerr angle θ vs. probe energy E_p. Pump energy is $E_0 = 1.58$ eV. (d) Hanle curves for different pump power densities. Solid lines represent fits to Eq. (2). The curves are shifted for clarity. (e) Hanle HWHM $B_{1/2}$ vs. pump power density W. The solid line is a fit to Eq. (3).

using $S_{z0} = 25\%$ (i.e., $\rho_{c0} = 12.5\%$) and a saturation pump power density $W_S = 8$ Wcm^{-2}. The net spin polarization is suppressed in a transverse magnetic field B due to the Hanle effect [1]. The Hanle curves we obtained for this sample are shown in Fig. 1(d). They are well described by the Lorentzian

$$S_z = \frac{S_z(W)}{1 + (B/B_{1/2})^2}\,. \qquad (2)$$

Here, $B_{1/2} = \hbar/(g_e\mu_B)T_s^{-1}$ is the halfwidth at half maximum (HWHM) of the Hanle curve given by the spin lifetime T_s connected with optical recombination. The Hanle HWHM $B_{1/2}$ increases with pump power density W as shown in Fig. 1(e). This behavior is well established for n-GaAs [1]. Upon increasing W, recombination with photogenerated holes provides an additional spin decay channel, resulting in a decrease of the spin lifetime given by [10]

$$B_{1/2} \propto T_s^{-1} = \tau_s^{-1}(1 + W/W_0)\,. \qquad (3)$$

Here, W_0 defines a characteristic pump power density, and the regime where $W > W_0$ implies strong spin pumping. In the low power density limit, T_s is equal to the spin relaxation time of electrons τ_s, and, using the well-known electron g-factor in GaAs ($g_e = -0.44$) our Hanle data yield an electron spin lifetime $\tau_s = 98$ ns [Fig. 1(e)].

The Hanle effect is also clearly observed in MOKE measurements. Figure 1(c) demonstrates the dependence of the Kerr angle θ on the probe energy E_p in zero magnetic field (solid line). Note that the Kerr angle completely vanishes at $B = 5$ mT (in the limit of low pump and probe density, dotted line). In the subsequent experiments, we measure the Kerr angle at a fixed energy of $E_p = 1.514$ eV (as indicated by the arrow).

We now describe our results obtained by Kerr microscopy, where the laser beams are focused tight enough to resolve spin diffusion. The spatial resolution of our

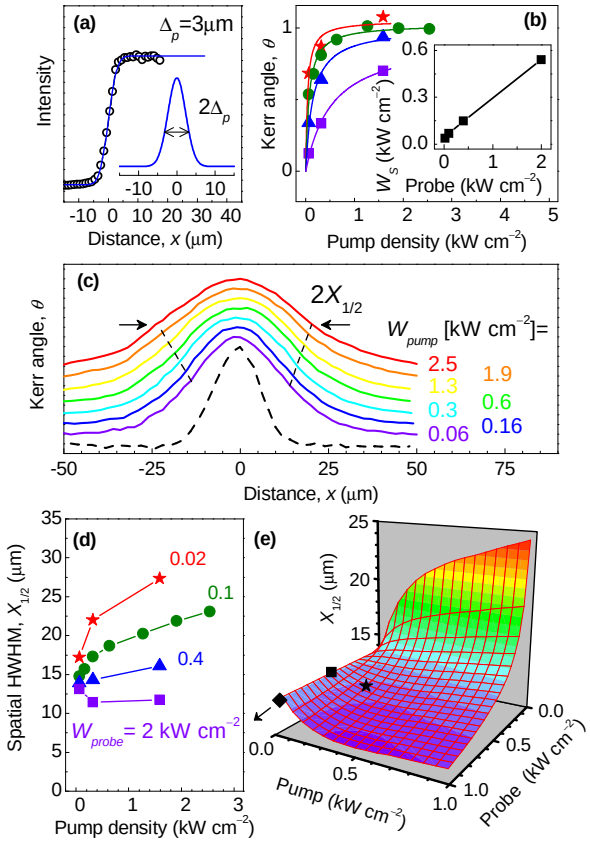

FIG. 2: (Color online) Spin pumping in the diffusive regime. (a) Scan of the laser spot through a sharp edge. Inset: laser spot profile. (b) Kerr angle at the center of the pump spot ($x = 0$) vs. pump power density for several probe power densities. Solid lines are fits to Eq. (1). Inset: saturation pump power density W_S vs. probe power density W_{probe}. (c) Spatial spin distribution for different pump power densities W_{pump}. The probe power density is $W_{probe} = 0.1$ kWcm^{-2}. The dotted curve gives the experimental resolution. (d) Spatial HWHM $X_{1/2}$ vs. pump power density for several probe power densities. (e) Overview of the 2D dependence of the spatial HWHM $X_{1/2}$ on pump and probe power density. Symbols indicate experimental conditions in various papers: ★ - Ref. 3, ■ - Ref. 7 and ♦ - Ref. 9.

setup can be inferred from a scan of the transmission of the focused laser beam over a sharp edge, as shown in Fig. 2(a). The derivative of this trace (inset) confirms that the spot profile has the form $\exp(-x^2/\Delta_p^2)$, with $\Delta_p = 3.3$ μm; we have verified that the profile in the sharp-edge scans is circular. Diffusion of optically injected spins causes the spatial profiles shown in Fig. 2(c). The dotted line in this figure shows the excitation profile as detected by the probe. It corresponds to the convolution of pump and probe spots and yields a net resolution of $\Delta = 7.5$ μm. The spatial HWHM $X_{1/2}$ of the scans in the Figure (and therefore the spin diffusion length $L_s = \sqrt{D_s \tau_s}$) is not constant, as one might naively anticipate, but rises from 14 μm for $W = 0.06$ kWcm^{-2} to 23 μm for $W = 2.5$ kWcm^{-2}. It seems unlikely that the spin relaxation time τ_s becomes longer with increasing spin pumping. Hence, we ascribe such a behavior to an increase of the spin diffusion constant D_s. This suggests that optically injected electrons not only provide a local spin source, but also participate in spin transfer over tens of microns. Note that a possible heating effect by light can be ruled out, as we observe a decrease of $X_{1/2}$ with rising bath temperature.

This effect is summarized for different probe power densities in Fig. 2(d). As a general trend, the spin diffusion length decreases with increasing probe power density. In order to examine the origin of such a behavior, we plot in Fig. 2(b) the Kerr rotation at the excitation point ($x = 0$) as function of pump power density for several probe power densities. These dependencies are well fitted by Eq. (1), where the fitting procedure reveals that also the saturation pump power density W_S depends on the probe power density, following a linear increase [see inset of Fig. 2(b)]. This makes intuitive sense: the faster the spin decay, the stronger spin pumping is required to achieve saturation. The probe beam generates holes, introducing an additional spin decay channel. The efficiency of this channel scales with the ratio of the spin relaxation time and the electron-hole recombination time, and it obviously is efficient even at moderate power density. As a consequence, the spin polarization is destroyed and the spin diffusion is suppressed for increasing probe power density. The overall dependence of the spin diffusion process on the pump and probe power density is summarized in Fig. 2(e). In this plot we have included the actual experimental conditions from various recent papers, labeled by symbols. While the influence of the power level used in these works is not very significant, these data have not been taken in the true low perturbation regime.

We now demonstrate how the above effect in combination with weak magnetic fields can be used to locally manipulate the spin flow around the excitation spot. A 2D spatial scan in the regime of strong spin pumping $W_{pump} \gg W_0$ ($W_{pump} = 1.6$ kWcm^{-2}) is shown in Fig. 3(a) for zero magnetic field. In order to minimize the influence of the probe light, its power density is reduced to $W_{probe} = 0.1$ kWcm^{-2}. When an external magnetic field is applied in the sample plane, the spatial spin distribution changes drastically [Fig. 3(b)]. As clearly seen in Fig. 3(c), the HWHM of the spatial profile $X_{1/2}$ decreases with increasing magnetic field and saturates for $B > 5$ mT at the resolution limit of $\Delta = 7.5$ μm resulting from the finite sizes of pump and probe spots.

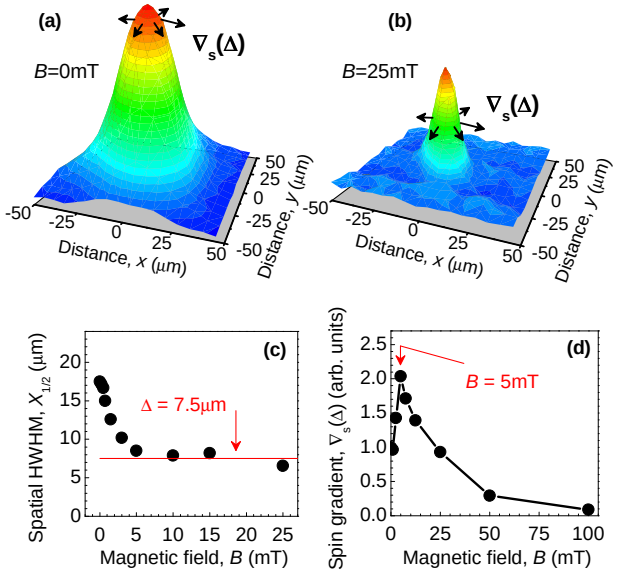

FIG. 3: (Color online) (a) Spatial spin distribution in zero magnetic field. (b) The same in a transverse magnetic field of 25 mT. (c) Spatial HWHM vs. magnetic field. (d) Spin gradient $\partial\theta/\partial x \propto \nabla_s$ obtained at a distance $x = \Delta$ vs. magnetic field. $W_{pump} = 1.6$ kWcm^{-2} and $W_{probe} = 0.1$ kWcm^{-2}.

Obviously, also the spin gradient $\nabla_s \propto \partial\theta/\partial x$ in Fig. 3 depends on the in-plane magnetic field. We now concentrate on the spin gradient at the point $x = \Delta$. It has a precise physical meaning: $\nabla_s(\Delta)$ is proportional to the spin flow emanating from the injection point due to the diffusion process. Hence, we plot in Fig. 3(d) $\partial\theta/\partial x$ obtained at $x = \Delta$ as function of the magnetic field. The data are normalized by their value in zero field. The spin gradient shows a non-monotonic behavior. For small magnetic fields it increases until its value has doubled, then it decreases towards zero in stronger fields. The maximum is achieved at $B = 5$ mT. This implies that the spin flow from the injection area is enhanced in weak in-plane magnetic fields.

In order to understand the origin of this effect, we have taken Hanle curves at various positions in the diffusion profile. These data are shown in Fig. 4(a). The small asymmetry of these curves results from the orientation of the optically generated spins under an angle $\gamma = 11°$ with respect to the sample normal (z-axis). At the generation point $x = 0$ μm a much higher magnetic field ($2B_{1/2} = 18$ mT) is required to suppress the spin polarization than in more distant locations ($2B_{1/2} = 6$ mT

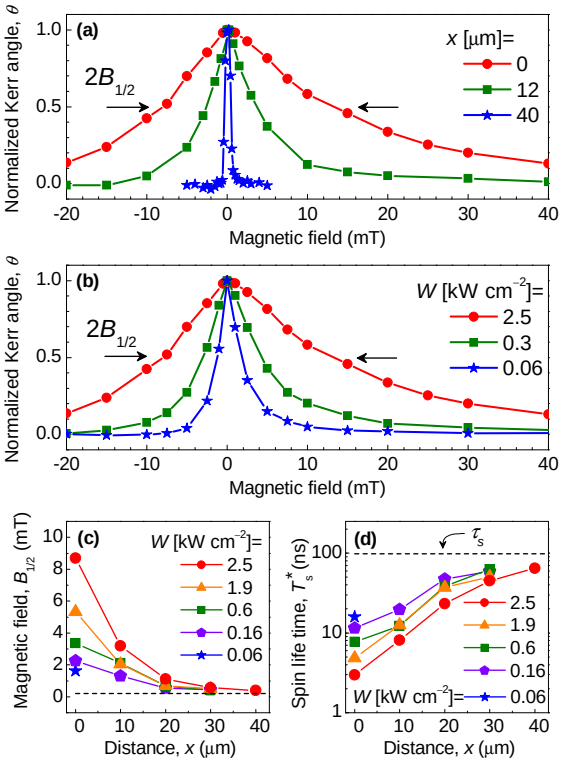

FIG. 4: (Color online) Spatially resolved Hanle effect obtained with $W_{probe} = 0.1$ kWcm^{-2}. (a) Local Hanle curves for different distances x. $W_{pump} = 2.5$ kWcm^{-2}. (b) Local Hanle curves for different pump power densities W_{pump}. $x = 0$ μm. (c) Spatial dependencies of $B_{1/2}$ for different pump power densities. (d) Spatial dependence of the apparent spin lifetime T_s^* for different pump power densities.

at $x = 12$ μm and $2B_{1/2} = 0.8$ mT at $x = 40$ μm). This strong spatial dependence of the spin lifetime actually scales with illumination power density. As shown in Fig. 4(b), when the pump power density decreases from $W_{pump} = 2.5$ kWcm^{-2} to $W_{pump} = 0.06$ kWcm^{-2} the width of the local Hanle curves detected at $x = 0$ also reduces from $2B_{1/2} = 18$ mT to $2B_{1/2} = 3.2$ mT.

The spatial dependencies of $B_{1/2}$ for different pump power densities are summarized in Fig. 4(c). Remarkably, when the detection point is far away from the injection point (for $x > 20$ μm), $B_{1/2}$ is nearly independent of the pump power and tends towards $B_{1/2} = 0.25$ mT, as obtained for low pump power densities in Fig. 1(e), where spin diffusion can be neglected.

The experimental results of Fig. 4(c) can be interpreted in terms of an apparent spin lifetime T_s^*. While the Hanle curves in the diffusive regime are not described by the Lorentzian of Eq. (2) [1, 2], also in this limit the width of the Hanle curves scales with the inverse of the spin lifetime [12]. Hence, we evaluate this apparent spin lifetime using $T_s^* = \hbar/(g_e\mu_B)B_{1/2}^{-1}$. The T_s^* values thus obtained are plotted in Fig. 4(d) as a function of the distance x for different pump power densities. These data clearly demonstrate that illumination induces a spatial variation of the spin lifetime.

Based on the results of Fig. 4 we propose the following physical explanation for the increase of spin flow at low magnetic field presented in Fig. 3(d): In zero field the optically generated spins S_z diffuse away to a distance of the order of the spin diffusion length L_s, resulting in a spin gradient $\nabla_s \propto S_z/L_s$. Outside of the injection area, photo-generated holes are absent and the spin lifetime entering Eq. (3) is equal to the electron spin relaxation time, $T_s^* \approx \tau_s$. Therefore, in relatively weak magnetic fields ($B \sim 5$ mT) the net spin polarization is completely suppressed in this region. Quite the opposite situation prevails inside the injection area when the condition of strong spin pumping ($W_{pump} \gg W_0$) is fulfilled. In this case $T_s^* \ll \tau_s$ and much higher magnetic fields are required to suppress the net spin polarization. As a result, the spin gradient increases in weak magnetic fields according to $\nabla_s \sim S_z/\Delta$. The enhancement factor can be estimated at L_s/Δ. In sufficiently strong magnetic fields the spin polarization inside the injection area is also suppressed ($S_z \to 0$) and the spin gradient decreases to zero. For low pump power densities ($W \ll W_0$) according to Eq. (3) $T_s^* \approx \tau_s$ and the spin gradient decreases spatially uniformly with increasing magnetic field, and the effect disappears.

Summarizing, we used scanning Kerr microscopy to reveal a strong influence of pump and probe on spin transport at the power levels which are frequently assumed to satisfy weak spin pumping conditions. We demonstrate that optical illumination induces spatial variations of the spin lifetime, which in turn can be used to locally control the spin flow when combined with a weak magnetic field. We have shown that the effect can be successfully harnessed to offer a novel possibility to manipulate spin currents.

The authors thank T. Kiessling for valuable discussions. This research was supported by the DFG (SPP 1285).

* Also at A. F. Ioffe Physico-Technical Institute, RAS, 194021 St. Petersburg, Russia;
E-mail: astakhov@physik.uni-wuerzburg.de

[1] *Optical Orientation*, edited by F. Meyer and B. P. Zakharchenya (North-Holland, Amsterdam, 1984).
[2] R. I. Dzhioev *et al.*, Phys. Solid State **39**, 1765 (1997).
[3] S. A. Crooker and D. L. Smith, Phys. Rev. Lett. **94**, 236601 (2005).
[4] M. Oestreich *et al.*, Appl.Phys. Lett. **74**, 1251 (1999).
[5] R. Fiederling *et al.*, Nature **402**, 787 (1999).
[6] Y. Ohno *et al.*, Nature **402**,790 (1999).
[7] S. A. Crooker *et al.*, Science **309**, 2191 (2005).
[8] P. Kotissek *et al.* Nature Phys. **3**, 872 (2005)
[9] Y. K. Kato, R. C. Myers, A. C. Gossard, and D. D. Awschalom, Science **306**, 1910 (2004).

[10] H. Hoffmann *et al.*, Phys. Rev. B **74**, 073407 (2006).
[11] S. A. Crooker *et al.*, J. Appl. Phys. **101**, 081716 (2007).
[12] M. I. Dyakonov and V. I. Perel, Fiz. Tekhn. Poluprovodn. **10**, 350 (1976).